Progestins counteract estrogens to shift breast cancer cells into a quiescent metabolic profile

Shawna Matthews
University of Colorado Denver - Anschutz Medical Campus
Lynsey M. Fettig
University of Minnesota
Ashley V. Ward
University of Colorado Denver - Anschutz Medical Campus
Jessica Finlay-Schultz
University of Colorado Denver - Anschutz Medical Campus
Peter Kabos
University of Colorado Denver - Anschutz Medical Campus
Matthew Jackman
University of Colorado Denver - Anschutz Medical Campus
Paul S. MacLean
University of Colorado Denver - Anschutz Medical Campus
Carol A. Sartorius (carol.sartorius@cuanschutz.edu)
https://orcid.org/0000-0002-9170-3988

Research

Keywords: Breast cancer, estrogen, progesterone, estrogen receptor, progesterone receptor, metabolism, mitochondria

Posted Date: February 17th, 2020

DOI: https://doi.org/10.21203/rs.2.23619/v1

Abstract

Background Progestins generally suppress the growth of estrogen receptor (ER) and progesterone receptor (PR) positive breast cancers and are occasionally used as treatments. However, progestins also increase populations of therapy-resistant cancer stem cells. We speculated that the downstream effects of progestins on cell metabolism might help explain its unusual impact on cell phenotype. Thus, in this study we investigated how progestins, in the absence or presence of estrogens, affect cell metabolism in ER+PR+ breast cancer. Methods Metabolites were quantified and compared from ER+PR+ breast cancer cell lines T47D and UCD65 treated with vehicle, estrogen only, progestin only, or the combination using ultra-performance liquid chromatography coupled with mass spectrometry (UPLC-MS). Metabolic flux analysis was performed on cells given the same hormone treatments. Likewise, the influence of treatments on mitochondrial morphology was measured using transmission electron microscopy in cell lines and patient-derived xenograft tumors and mitochondrial-targeted GFP in cell lines. Mitochondrial biogenesis was measured via fluorescence shift in the photoconvertible MitoTimer reporter coupled with confocal microscopy, and biogenesis regulators were measured by qPCR. Select metabolites and ATP were measured using fluorometric assays. Results Estrogen plus progestin treatment largely reverses estrogen-stimulated metabolic activities in breast cancer cells including increased TCA cycle metabolites, amino acid metabolism, and glutathione metabolism. Addition of progestins to estrogen impaired mitochondrial oxygen consumption and ATP production of cancer cells. Moreover, while estrogen-treated cells had elongated mitochondrial morphology, progestin co-treatment resulted in a more aged and less elongated mitochondrial population. Notably, progestins blocked the estrogen-induced expression of mitochondrial biogenesis regulators PGC1α and PGC1β and their downstream targets. While progestin treatment reduced total intracellular amino acid and glutathione pools, a subpopulation of progestin-inducible cancer stem cells revealed a dependence on glutathione. Conclusions These findings indicate that progestins antagonize estrogen’s effects on cellular metabolism and shift cells to a more quiescent phenotype, with reduced mitochondrial functional capacity, more reliance on glycolysis, and increased cell survival traits. Our results have implications for current clinical studies testing selective PR modulators in ER+ breast cancers.

Background

In the normal breast, the female hormones estrogen and progesterone act in coordination to facilitate growth and development. In breast cancer, however, hormone signaling becomes aberrant and uncoupled from its normal tissue function. Nearly three-quarters of breast cancers are estrogen receptor alpha (ER) positive and depend on estrogens for growth (1). As most diagnoses occur in postmenopausal women with low circulating estrogen levels, tumor growth in these women relies on local adipose tissue production of estrogen (2, 3). Progesterone dissipates more completely at menopause (4), and its reintroduction in hormone therapy (HT) with synthetic analogs (progestins) in combination with estrogens increases breast cancer incidence (5). However, as a treatment in advanced breast cancers, progestins have response rates similar to endocrine therapies such as tamoxifen and are sometimes

used upon endocrine failure (6–8). The dichotomy of action of progestins in the biology of breast cancer cells remains an impediment to their guided use in treatments.

Receptors for estrogens and progestins, ER and PR, are closely related members of the nuclear receptor transcription factor family. Crosstalk between family members is emerging as prototypical in controlling gene regulation and cell phenotype (reviewed in (9)). Proteomic and genomic studies in ER + PR + breast cancer cell lines and patient-derived xenografts (PDX) have found that unliganded PR is a cofactor in the ER transcription complex, and that progestins redirect ER-PR chromatin binding away from core estrogen responsive genes (10–12). Thus, transcriptional interference of ER driven genes is one mechanism by which PR suppresses the mitogenic activities of ER (10–12). However, the downstream consequences of ER-PR crosstalk on breast cancer cell physiology, particularly cellular bioenergetics and metabolism, are relatively unexplored. Understanding these changes is important since cancer cells adopt distinct metabolic phenotypes that modulate their longevity and survival (reviewed in (13)).

Estrogens stimulate breast cancer cell metabolism to satisfy the increased energy and biomass needs of growing cells. Energy-generating capacity for processes of oxidative phosphorylation (oxphos) and glycolysis is generally enhanced in the presence of estrogen through genomic and non-genomic mechanisms (reviewed in (14, 15)). Estrogen upregulates glucose transporters GLUT-1, -3, and − 4, and increases glucose uptake and consumption along with lactate production in breast cancer cells and xenografts (16, 17). Glutamine uptake and consumption also increases with estrogen treatment of ER + MCF7 breast cancer cells (18). Tricarboxylic acid (TCA) cycle enzymes including citrate synthase (12), aconitase (19), and isocitrate dehydrogenase are all increased by estrogen (20, 21). Likewise, estrogen treatment increases expression of mitochondrial-encoded electron transport chain subunits, including increased NADH dehydrogenase subunit 1 (ND1) and cytochrome oxidases I and II (COI, COII) (22–24). Both ERα and ERβ can localize to the mitochondrial matrix in the estrogen-responsive cell line MCF7 (25, 26). Collectively, ER targets bioenergetics processes with a notable impact on mitochondrial adaptation to meet the demands of continuous breast cancer cell growth.

In contrast to E2, progestin effects on breast cancer cell metabolism are less studied. PR regulates genes involved in cholesterol and steroid, fatty acid and lipid, and nucleotide and amino acid metabolism (27). In breast cancer cells, progestins increase de novo lipid synthesis and accumulation of lipid droplets (28). A truncated isoform of PR (mPR) was also reported to localize to the mitochondria of both ER + and ER − breast cell types, with proposed effects on mitochondrial membrane potential and functional capacity; however, the biological importance of mPR in cells with functional nuclear PR is unclear (29, 30). These few studies were done in the absence of estrogens and/or in ER − breast epithelial cells. The impact of progestins on estrogen-driven metabolism in ER + PR + breast cancer cells remains largely untested, while highly relevant since it represents the typical physiological and clinical context.

In this study, we evaluated the effect of estrogens, progestins, and the combination on modulation of cell metabolism machinery in ER + PR + breast cancer cells. We found that progestins perturb estrogen-driven mitochondrial metabolism by suppressing mitochondrial oxidative respiratory capacity and preventing

estrogen-induced mitochondrial elongation. This likely occurs by blocking mitochondrial biogenesis regulators. Overall, we conclude that progestins exert a dominant effect on estrogen-driven energy production in breast cancer cells, prospectively as part of a broader strategic shift from rapid tumor growth to cytostasis and metabolic dormancy. The consequences of a progestin-induced metabolic shift are unclear, but could have implications for the safety and efficacy of progestin-based breast cancer therapies.

Methods

Cell lines and cell culture

The breast cancer cell line T47D (ER + PR+) was obtained from the University of Colorado Cancer Center Tissue Culture core and was maintained in minimal Eagle's medium, 5% fetal bovine serum (FBS), 1X non-essential amino acids, 1×10^{-9} M insulin, 0.1 mg/mL sodium pyruvate, and 2 mM L-glutamine. Development of ER + PR + breast cancer PDX UCD4 and UCD65 has been previously described (12, 31). The UCD65 cell line was derived from the UCD65 PDX and is ER + PR + and Her2 unamplified. The UCD65 cell line was maintained in DMEM/F-12 1:1 with 10% FBS, 1×10^{-9} cholera toxin, 1×10^{-9} hydrocortisone, and 1×10^{-9} M insulin. Cell lines were authenticated using short tandem repeat (STR) analysis using the University of Colorado Genetics core. For UCD65, cells were matched to the original PDX and not to any other cell lines in the database. All cell lines were routinely tested for mycoplasma contamination using the MycoAlert mycoplasma detection kit (Lonza, Basel, Switzerland).

In vitro hormone experiments were performed using phenol red-free media with the same additives described above. Hormone treatment was used as follows: E2 = 17-β-estradiol, 10^{-8} M (Sigma-Aldrich, St. Louis, MO); P = R5020, 10^{-8} M (PerkinElmer, Waltham, MA). PR expression was induced in UCD65 cells by E2 pre-treatment for a minimum of 24 h prior to experiment start.

Animal Experiments

For these experiments, PDX tumors were partitioned into female NOD/SCID/ILIIrg$^{-/-}$ (NSG) mice supplemented with subcutaneous silastic pellets containing E2 or E2 + progesterone (P4) (called E2 + P herein) (Sigma-Aldrich, St. Louis, MO) as described previously (32, 33). For T47D xenografts, 1×10^{6} cells were injected into the mammary fat pad of female NSG mice supplemented with E2 or E2 + P pellets. Tumors were measured weekly with a digital caliper and volume was estimated by the formula $lw^2/2$. All animal experiments were performed under a protocol approved by the University of Colorado Institutional Animal Care and Use Committee.

Metabolomics

Metabolites were extracted from T47D and UCD65 cell pellets in quadruplicate using ice-cold extraction buffer (5:3:2 methanol:acetonitrile:water) at a concentration of 2×10^6 cells per mL as previously described (34, 35). Supernatants (10 uL) were analyzed on a Thermo Vanquish ultra-high performance liquid chromatography column coupled online to a Thermo Q Exactive mass spectrometer (UHPLC-MS) in positive and negative ion modes (separate runs) using a 5 min C18 gradient. Untargeted data acquisition, quality control, and targeted data analysis were performed as previously described (36). Precipitated protein was reconstituted in PBS and measured using BCA protein assay (Pierce, Thermo Fisher, Waltham, MA). Metabolomics intensity signals were normalized to sample protein concentration.

Normalized data was imported into MetaboAnalyst software (37, 38), where data was log-tranformed and autoscaled (39). Partial least squares discriminant analysis (PLS-DA) was performed on all samples within cell lines for visual inspection of clustering patterns and outlier detection. Heatmaps were constructed using Pearson distance with average linkage and depict non-scaled PLS-DA variable importance in projection (VIP) averaged across replicates (N = 4) within treatment groups.

For pathways analysis, pairwise comparisons were used: 1) vehicle-treated cells (Veh, 0.2% ethanol) vs. P-treated cells, and 2) E2-treated cells vs. E2 + P-treated cells. Metabolites from random forest variable importance analysis with mean decrease in accuracy > 0 were evaluated for fold-change direction (lower in E2 + P vs. E2, called “down”; higher in E2 + P vs. E2, called “up”). These subsets of metabolites were submitted to MetaboAnalyst Pathways Analysis (MetPA) and can be found in Additional file 1: Table S1 for T47D cells and Additional file 2: Table S2 for UCD65 cells. Pathways were identified using default settings; specifically, the hypergeometric test for overrepresentation analysis and relative betweenness centrality was used for pathway topology analysis, with pathways mapped to the Homo sapiens KEGG reference library.

Immunocytochemistry

Immunohistochemistry and ICC were performed as previously described (31, 40). Cells were plated on coverslips and fixed in methanol/acetone. The primary antibody directed against CK5 (#NCL-L-CK5, Leica Biosystems, 1:200) was applied for 1 hour followed by Alexa Fluor 488 goat anti-mouse fluorescent secondary antibody (#A11029, Thermo Fisher, Waltham, MA), counterstained with DAPI and mounted. Images were collected using a Nikon TiE microscope equipped with a digital camera and NIS Elements software.

Seahorse Metabolic Phenotyping

Metabolic phenotype was determined using the Seahorse XFe96 Extracellular Flux Analyzer (Agilent, Santa Clara, CA). Cells were cultured in the presence of hormones for 24–48 hours and assessed via the Mito Stress Test kit. Samples were analyzed with 5–6 replicates per treatment.

Atp Assay

Intracellular ATP was quantified using the ATP Fluorimetric Assay from Novus Biologicals (#NBP2-54855, Biotechne, Cambridge, MA) according to the manufacturer's protocol. Briefly, cells treated with hormones for 24, 48 h, or 72 hours were lysed in ice-cold assay buffer and deproteinized using the Deproteinizing Sample Preparation Kit (#K808-200, BioVision, LLC, Milpitas, CA) according to the manufacturer's protocol and assayed under fluorimetric conditions (Ex 535/Em 587) in triplicate. Results are representative of at least 3 experiments.

L-amino Acid Assay

Amino acids were measured using the L-Amino Acid Quantitation Kit (#MAK002, Sigma-Aldrich, St. Louis, MO) according to the manufacturer's protocol. Briefly, T47D cells treated with hormones for 24 h were homogenized in ice-cold assay buffer, diluted within linear range of the assay, and colorimetric absorbance at 570 nm measured in triplicate. Results are representative of at least 2 experiments.

Glutathione Assay

Intracellular glutathione (GSH) was quantified using the Glutathione Assay Kit from Cayman Chemicals (#703002, Ann Arbor, MI) according to the manufacturer's protocol. Briefly, T47D cells were treated with hormones for 24 h, lysed in ice-cold assay buffer, and deproteinized using the Deproteinizing Sample Preparation Kit (#K808-200, BioVision, LLC, Milpitas, CA). Deproteinated samples were measured for total glutathione (combined GSH + GSSG) via absorbance at 405 nm in triplicate. Results are representative of at least 3 experiments.

Inhibition Of Glutathione Synthesis

The small molecule buthionine sulfoximine (BSO) inhibits the catalytic subunit of the glutamate-cysteine ligase enzyme (GCLC), which catalyzes the rate-limiting step in glutathione synthesis (41). BSO was purchased from Cayman Chemical (#14484, Ann Arbor, MI) and was reconstituted fresh in sterile PBS immediately prior to use at a final concentration of 10^{-4} M.

Transmission Electron Microscopy

Cells were cultured on PermaNox 60-cm dishes (VWR, Radnor, PA). Excised tumors were cut into approximately 1 mm^3 pieces. Cultured cells and tumor pieces were fixed with 2% paraformaldehyde and 2.5% glutaraldehyde in 0.1 M phosphate buffer and then post-fixed with reduced osmium (1.5% potassium ferrocyanide + 1% osmium tetroxide) followed by 2% osmium tetroxide. Samples were dehydrated with a graded series of ethanol and embedded in a thin layer of Epon. Following Epon curing,

small pieces were cut out and re-embedded in blocks that were sectioned at 65 nm on an ultramicrotome, collected on formvar coated slot grids, and post-stained with 2% osmium tetroxide and lead citrate.

At least 10 fields per treatment were imaged and blinded prior to analysis. Mitochondrial length along the longest axis was measured using Fiji and plotted via histogram, with bin mode indicated on the X-axis. Outliers greater than 3 standard deviations outside the mean of the full dataset were excluded. Differences in distributions were analyzed using the Kolmogorov-Smirnov test for frequency distributions; comparisons for cells were 1) vehicle vs. E2 and 2) E2 vs. E2 + P, while tumor samples were pooled by hormone treatment and compared E2 pellets vs. E2 + P pellets.

Confocal Microscopy

T47D cells were labeled overnight with CellLights BacMam 2.0 MitoGFP (Thermo Fisher, Waltham, MA) according the manufacturer's protocol. Following treatment, cells were fixed in 4% paraformaldehyde, counterstained with DAPI, and mounted on coverslips. Images were collected using confocal laser scanning microscopy (Zeiss LSM 780) with 40X objective.

Mitotimer

T47D and UCD65 cells were transduced to express the MitoTimer construct from Addgene (Watertown, MA) as previously described (42). Following stable transduction with the pLenti-CMV-rtTA3 Blast (w756-1) (Plasmid #26429) with > 2 weeks blasticidin selection, cells were transiently transfected with pTRE-Tight-MitoTimer (Plasmid #50547) using Lipofectamine 3000 (Thermo Fisher, Waltham, MA). MitoTimer expression was induced by treatment for 1 hour with doxycycline (4 ug/ml, Cayman Chemical, Ann Arbor, MI), followed by washout and hormone treatment for 48 h, at which point most mitochondria should be yellow to red. A second 1 h dox pulse, followed by washout, was used to label a new wave of mitochondria corresponding to cells undergoing active biogenesis. Following an additional 6 h of hormone treatment, live cells (via IncuCyte ZOOM at 20X magnification or fixed cells (4% paraformaldehyde with DAPI counterstain) were imaged for analysis.

Real-time Quantitative Pcr (qpcr)

RNA was harvested using QIAzol lysis reagent (Qiagen, Venlo, the Netherlands) and converted to cDNA using the Verso cDNA kit (Thermo Fisher, Waltham, MA). qPCR was performed on cDNA using ABsolute Blue Sybr Green (Thermo Fisher, Waltham, MA) and normalized to β-actin using the Pfaffl method (43). qPCR primers are provided in Additional file: Table S3. Results are representative of 3–4 experiments.

Statistical Analyses

Statistics were performed using GraphPad Prism 8.3.0 (GraphPad Software, San Diego, CA), with the exception of metabolomics data, which was analyzed using MetaboAnalyst (see Metabolomics section for details). Two-tailed Student's t-tests, or one-way ANOVA followed by Tukey post hoc multiple comparison tests were used as indicated with significance set a priori at $P < 0.05$. Equivalent non-parametric tests were used in the event of unequal variance between groups.

Results

Progestins counter-regulate estrogen-driven metabolic reprogramming

To globally evaluate the combined effects of estrogen plus progestin on the bioenergetics of breast cancer cells, we performed metabolomics on two ER + PR + breast cancer cell lines (T47D and PDX-derived cell line UCD65) treated with vehicle (Veh), estrogen (17β-estradiol, E2), the synthetic progestin R5020 (P), or combination (E2 + P) for 24 h. The four treatment groups were readily distinguished based on their metabolite signatures, with E2 treatment causing a notable metabolic shift in both cell lines (Fig. 1A and 1B). Heatmaps of the top 50 features by variable importance (VIP) scores demonstrated wide-scale reductions in metabolites in cells treated with P, either alone or in combination with E2 (Fig. 1C and Fig. 1D).

We used MetaboAnalyst Pathways Analysis (MetPA) to identify the most significant pathways altered in T47D and UCD65 cells, shown in Fig. 1E. We focused our analysis on E2 vs. E2 + P which captures the most common physiological scenario. In both cell lines, many metabolic pathways were down-regulated in E2 + P compared to E2, including the TCA cycle, amino acid metabolism, and the glutathione antioxidant defense pathways. Only the pentose phosphate pathway was stimulated by E2 + P vs. E2. These results suggest P may impact the overall energetic phenotype of estrogen-driven cells in a manner consistent with the preferential use of carbohydrates for glycolytic energy production.

Progestins Shift Cells To A More Quiescent Bioenergetic Phenotype

Since TCA cycle was a key affected pathway in each cell line, we speculated that a reduction in TCA cycle metabolites might indicate a shift in the energetic profile. Seahorse flux analysis revealed that hormone treatment of T47D and UCD65 cells altered the basal usage ratio of oxphos to glycolysis, called 'energetic phenotype' (Fig. 2A). When mitochondrial stress was induced by inhibiting ATP synthase (oligomycin) and uncoupling membrane potential (FCCP), the combination of E2 + P significantly decreased the maximal oxygen consumption rate (OCR) compared to E2 alone with no compensatory change in glycolysis. Thus, in both cell lines, E2 + P effectively shifted cells from an "Energetic" phenotype, with high oxphos/high glycolysis, toward a "Quiescent" phenotype, with lower oxphos/lower glycolysis. In T47D but not UCD65 cells, E2 + P treatment reduced maximal respiratory capacity compared to P alone and

compared to vehicle, suggesting that combined hormone treatment may exert a greater effect on respiratory capacity than either hormone alone (Fig. 2B).

In agreement with observed changes to energetic phenotype, we observed a time-dependent increase in ATP with E2 treatment, increasing to approximately 140% or 125% of Vehicle-treated ATP by 72 h in T47D and UCD65 cells, respectively (Fig. 2C). P alone did not impact ATP in either cell line. The E2 dependent ATP increase in intracellular ATP was significantly blocked by combination E2 + P in T47D and trended downward in UCD65 cells (P = 0.056) (Fig. 2C) These data suggest that P co-treatment blocks the E2-driven increase in energy production.

Progestin Co-treatment Blocks E2-driven Mitochondrial Elongation

As functional assays suggested that P might be targeting mitochondrial function, we evaluated mitochondrial morphology using transmission electron microscopy (EM) in T47D and UCD65 cells (Fig. 3A). E2 treatment increased mitochondrial axis length whereas mitochondria treated with E2 + P were similar to vehicle, suggesting that P blocked the elongating effect of E2 (T47D cells, mode: E2 + P = 400 nm; Veh, P = 500 nm, E2 = 700 nm; UCD65 cells, mode: Veh, E2 + P, P = 300 nm; E2 = 400 nm) (Fig. 3B). To determine if this effect persisted in vivo in the context of solid tumors with chronic treatment with natural progesterone (P4), EM analysis of T47D xenografts and ER + PR + UCD4 PDX tumors was performed. The analysis revealed that mitochondria from cancer cells grown in mice supplemented with E2 were generally more elongated than in mice supplemented with E2 + P4 (T47D tumors, mode: E2 + P tumors 1,2 = 300; E2 tumors 1,2 = 500 nm; UCD4 tumors, mode: E2 + P tumor 1, 300; E2 + P tumor 2, E2 tumor 1 = 400 nm; E2 tumor 2 = 500 nm) (Fig. 3C and Fig. 3D). These data support that co-treatment with E2 + P versus E2, in cell lines and tumors, shifts mitochondria to a less elongated phenotype, which is consistent with lower functional capacity and reduced oxidative activity (44).

Progestin-treated Cells Have A More Aged Mitochondrial Network

To visualize the entirety of the mitochondrial network within cells, mitochondria labeled with a baculovirus GFP construct demonstrated that cells treated with E2 had enhanced phenotypic mitochondrial signal compared to cells treated with E2 + P (Fig. 4A). We speculated that P may activate mitochondrial fission to block effects of E2; however, we did not find evidence of activated fission with P treatment, determined by qPCR for fission proteins and Western blot for total dynamin-related protein (Drp-1) and its phospho-Ser^{616} isoform, which represents activated Drp-1 (Additional file: Fig. S1).

Therefore, we evaluated mitochondrial turnover to interrogate processes of mitochondrial birth (biogenesis) and death using the inducible MitoTimer system developed by Hernandez et al (42), in which

newly made mitochondria fluoresce green but photoconvert to red fluorescence over approximately 48 h. Confocal microscopy revealed that the majority of mitochondria in E2-treated cells were green and yellow, indicative of continual mitochondrial biogenesis, whereas mitochondria from P or E2 + P-treated cells were relatively more orange or red, indicative of older mitochondria (Fig. 4A). Quantitation of MitoTimer demonstrated an increased ratio of green:red fluorescence (more cells with predominantly green “new” mitochondria than red “old”) with E2 treatment (Fig. 4B). When cells were classified as having predominantly red, green or yellow mitochondria, E2 treated cells had a higher proportion of predominantly green mitochondria, whereas P treated cells had a striking reduction in cells with green mitochondria and a gain in cells with predominantly red mitochondria (Green % cells: Veh = 20%; E2 = 27%; P = 8%; E2 + P = 15%; red % cells: Veh = 40%; E2 = 40%; P = 52%; E2 + P = 39% [P for table = .026]) (Fig. 4C).

Progestins Block The E2-induced Pgc1α Mitochondrial Biogenic Signaling Cascade

Mitochondrial biogenesis is regulated by the peroxisome proliferator activated receptor gamma coactivator (PGC) family of proteins, particularly PGC1α. Since P treatment resulted in a more aged mitochondrial network, we evaluated the mitochondrial biogenesis signaling cascade depicted in Fig. 5A for response to hormone treatment. E2 increased transcript expression of Nrf2 (NFE2L2) (Fig. 5B) and its downstream targets PGC1α (PPARGC1A) (Fig. 5C) and PGC1β (PPARGC1B) (Fig. 5D). Conversely, the time-dependent induction of PGC1α by E2 was entirely mitigated by co-treatment with P; this was observed to a lesser extent in PGC1β. Downstream effectors of PGC1α include the Nrf1 (NFE2L1) transcription factor and mitochondrial transcription factor A (TFAM) which activate mitochondrial biogenesis and trigger replication of the mitochondrial genome, respectively. E2 induction of these targets was abolished by E2 + P treatment (Fig. 5E and Fig. 5F, respectively). This reduction in transcript levels of key mitochondrial biogenesis genes in response to progestin co-treatment, with the exception of PGC1β, was largely recapitulated in UCD65 cells (Additional file: Fig. S2). Detection of PGC1α protein level is complex, due to the presence of more than 10 isoforms with variable stability, biological activity, and tissue expression (45). However, immunoblot against Nrf2 as the inducer of the downstream signaling cascade suggested a decrease in Nrf2 protein expression with P alone or E2 + P (Additional file: Fig. S3).

Figures 1–5 demonstrated that P co-treatment slows cell metabolism compared to E2 alone: by lowering oxphos, progestins shift cells to a glycolytic energy profile. While this shift could be favorable for a quiescent cytostatic phenotype, it could also potentially prolong cancer cell survival. To evaluate other potential metabolic contributors to cytostasis, we returned to our initial metabolomics findings to interrogate amino acid regulation and the glutathione pathway, both shown to be down-regulated in E2 + P vs. E2 alone.

Subpopulations Of Progestin-treated Cells Demonstrate Divergent Glutathione Dependence

Beyond their role as metabolic substrates for the TCA cycle and protein biosynthetic precursors, amino acids play a key role in other cellular signaling cascades, including redox homeostasis. We used biochemical assays to validate our metabolomics findings of progestin effects on intracellular amino acids and glutathione. Co-treatment with progestins elicited a striking reduction in the L-amino acid pool compared to E2 alone (Fig. 6A). Likewise, we validated a reduction in the total glutathione pool in response to progestin treatment (Fig. 6B).

As many types of chemotherapy exert cytotoxicity via induction of oxidative stress, we found the limited glutathione defense capacity of progestin-treated cells intriguing from a potential therapeutic perspective. We and others have shown that both natural and synthetic progestins induce a subpopulation of cells to acquire cancer stem cell (CSC) properties including relative quiescence, tumorsphere formation, increased tumor initiating capacity, and resistance to endocrine and chemotherapies (46–50). Progestin-inducible CSCs lose expression of ER and PR while activating expression of the basal cytokeratin, cytokeratin 5 (CK5) (46). As glutathione is a vulnerability of many types of CSCs (eg, (51–53)), we used the small molecule buthionine sulfoximine (BSO) to block the rate-limiting step in glutathione synthesis. As shown in Fig. 6C and quantified in Fig. 6D, P treatment induces approximately 15% of T47D cells to express CK5. Upon co-treatment with P + BSO, the CK5 subpopulation is largely absent, suggesting that targeting the glutathione dependency of P-inducible CSCs may be a viable strategy to mitigate one negative consequence of P treatment.

Together these data suggest that P, alone or in combination with E2, antagonizes mitochondrial respiration to shift the energetic potential of ER + breast cancer cells towards a low-energy more quiescent phenotype with reduced mitochondrial activity. Since these cells are cytostatic yet viable, the consequence and permanence of the metabolic dormancy remain key questions.

Discussion

Disruption of normal metabolic pathways is a hallmark of cancer. In the majority of breast cancers, aberrant estrogen signaling drives metabolic changes. This is the first study to our knowledge that demonstrates progestins antagonize the metabolic effects of estrogen, including inhibition of ATP production, disruption of mitochondrial function and biogenesis, and depression of amino acid levels for reduced anabolic capacity. Concurrently, progestins alter the cell's antioxidant defense system through the glutathione pathway, another important hallmark of cancer and cell survival. These findings have implications for pre- and postmenopausal women taking progestins for HT and breast cancer treatments.

It is well established that synthetic progestins in combination with estrogen are tumorigenic in women without a history of breast cancer. A 2019 meta-analysis by the Collaborative Group on Hormonal Factors in Breast Cancer confirmed increased breast cancer risk with nearly every type of synthetic progestin

containing HT compared to estrogen-only HT (5). Some theories suggest progestins activate pre-existing occult cancer stem cells in these women (54, 55). In fact, it is well known that in established breast cancer models, progestins increase populations of cancer stem cells, while slowing overall cell/tumor growth (eg, (12, 46, 49, 50)). Interestingly, both quiescence and stem cell maintenance require low cellular energy production. In normal tissues, embryonic and induced pluripotent stem cells generally fulfill energy needs through glycolysis while differentiation reduces glycolytic rate with increased oxphos (56). Energetic processes in CSCs, where defined, depend on tumor type and show considerable metabolic plasticity (reviewed in (57)). Given the unique hormone dependency of most breast cancers, CSC metabolism is likely to be influenced by hormonal milieu.

In our studies, progestins had a profound impact on mitochondrial morphology and function. First, progestins changed the energetic phenotype of cancer cells by suppressing oxphos while maintaining glycolysis (Fig. 2), suggesting that progestin treatment reduces mitochondrial activity. Second, progestins notably altered mitochondrial morphology (in the absence or presence of estrogens) transitioning to less elongated mitochondria (Fig. 3, Fig. 4). Mitochondrial morphology is tightly linked to energy metabolism: a highly inter-connected mitochondrial network and enlarged cristae are associated with enhanced respiration, whereas low oxphos and high glycolysis correlates with smaller mitochondria displaying reduced intracristae space (58). Furthermore, disrupting or modulating mitochondrial dynamics can have profound impacts on stem cell behaviors (59). For example, deletion of PGC-1α and PGC-1β in pre-adipocytes prevents their differentiation into mature adipocytes, whereas stimulation of mitochondrial biogenesis promotes differentiation of embryonic stem cells and induced pluripotent stem cells (59). Curiously, progestins potently decreased PGC1α and PGC1β in breast cancer cells (Fig. 5, Additional file: Fig. S2). We speculate this in addition to regulation by other genes contributes to the observed switch in mitochondrial phenotype and function. Whether this progestin-induced metabolic response is transient or persistent will be important to know, since a recent meta-analysis found that tumors expressing high levels of glycolytic proteins were more aggressive and corresponded to shorter overall survival of breast cancer patients, as well as other types of cancer (60).

The metabolic phenotype of cancer cells that have been forced into cytostasis is virtually untested. Studies by Havas et al (61), using primary murine mammary organoid cultures with inducible oncogene expression noted metabolic shifts in residual cells following oncogene withdrawal that were important for recurrence. Noticeably, many of the pathways identified by Havas as distinct between induced vs. regressed organoids overlapped with metabolic pathways we identified as counter-regulated by E2 + P vs. E2 including reduced aminoacyl-tRNA biosynthesis, TCA cycle, glyoxylate/ dicarboxylate metabolism, and Ala/Asp/Glu metabolism (61). Progestin and endocrine therapies induce a cytostasis that is thought to keep occult tumor cells dormant for long duration or even permanently. Neither cytostasis, nor the factors that trigger exit from dormancy, are well understood and it is conceivable that manipulation of the described progestin induced metabolic profile could act as a treatment target. Interestingly, Havas found that PR antagonists reduced recurrence of their organoid models upon re-induction of oncogenes (61). This has relevance to ongoing studies of PR agonists and antagonists for treatment of ER + breast cancer, and which types of ligands are able to reduce growth and prevent recurrence.

In conclusion, our studies support that progestins induce a metabolic transition in ER + breast cancer cells away from oxphos towards a glycolytic and stress-avoiding phenotype. We speculate that this shift is important for the dual actions of progestins in subduing estrogen-driven growth and promoting expansion of CSCs. Furthermore, our studies emphasize that the type and duration of progestin use is similarly important for breast cancer treatment as it is for HT. Further studies into hormone-regulated metabolic phenotypes may help design strategies to prolong benefits of relatively non-toxic PR targeted therapies.

Conclusions

Our understanding of the metabolic phenotype of hormone-dependent breast cancer cells is limited, particularly in relation to estrogens, the underlying driver, and progestins, often used in medicines and treatments. Here we report that progestins impair estrogen-induced energy production by disrupting the function of existing mitochondria and blocking creation of new mitochondria. Progestins cause breast cancer cells to undergo a metabolic switch from a high-energy mitochondria-powered phenotype to a low-energy glycolysis-powered phenotype. Additionally, we find that a key intracellular stress manager, the glutathione pathway, is altered by progestins and may help sustain a subpopulation of treatment-resistant cancer cells. Our work has implications for progestins and antiprogestins that are being tested in clinical trials, suggesting that immediate benefits may be counteracted by long term adeptness of cytostatic cells. Furthermore, some identified features could be potential vulnerabilities of progestin treated cells.

Abbreviations

ANOVA
Analysis of variance
ATP
Adenosine triphosphate
BCA
Bicinchoninic acid
BSO
Buthionine sulfoximine
cDNA
Complementary DNA
CK5
Cytokeratin 5
COI
Cytochrome oxidase I
COII
Cytochrome oxidase II

CSC
Cancer stem cell
DAPI
4',6-Diamidino-2-phenylindole
DMEM
Dulbecco's modified Eagle's medium
DNA
Deoxyribonucleic acid
Dox
Doxycycline
Drp-1
Dynamin-related protein, DNM1L
E2
17-β-estradiol
ECAR
Extracellular acidification rate
EM
Electron microscopy
ER/ ERα
Estrogen receptor alpha, ESR1
ERβ
Estrogen receptor beta, ESR2
FBS
Fetal bovine serum
GCLC
Glutamate-cysteine ligase, catalytic subunit, GCLC
GFP
Green fluorescence protein
GLUT
Glucose transporter protein family
GSH
Reduced glutathione
GSSG
Oxidized glutathione
HER2
Human epidermal growth factor receptor 2, ERBB2
HT
Hormone therapy
ICC
Immunocytochemistry

KEGG
Kyoto Encyclopedia of Genes and Genomes
MetPA
MetaboAnalyst Pathways Analysis
mPR
Putative mitochondrial PR
NADH
Nicotinamide adenine dinucleotide
ND1
NADH dehydrogenase subunit 1
Nrf1
Nuclear factor erythroid 2-like 1, NFE2L1
Nrf2
Nuclear factor erythroid 2-like 2, NFE2L2
NSG
NOD/SCID/ILIIrg$^{-/-}$ mice
OCR
Oxygen consumption rate
Oxphos
Oxidative phosphorylation
P
Synthetic progestin R5020
P4
Natural progesterone
PBS
Phosphate-buffered saline
PDX
Patient-derived xenograft
PGC1α
PPAR-gamma coactivator alpha, PPARGC1A
PGC1β
PPAR-gamma coactivator beta, PPARGC1B
PLS-DA
Partial least squares discriminant analysis
PPAR
Peroxisome proliferator activated receptor
PR
Progesterone receptor, PGR
qPCR
Quantitative real-time polymerase chain reaction

RNA
Ribonucleic acid
STR
Short tandem repeat
TCA
Tricarboxylic acid
tRNA
Transfer RNA
UCD
University of Colorado Denver; prefix for PDX-derived tumors and cell lines
UHPLC-MS
ultra-high performance liquid chromatography coupled with mass spectrometry
Veh
Vehicle for hormone treatment, ethanol
VIP
Variable importance in projections

Declarations

Ethics approval and consent to participate

All animal experiments were approved by the University of Colorado Institutional Animal Care and Use Committee (#00160) and conducted in accordance with their guidelines.

Consent for publication

Not applicable.

Availability of data and materials

The metabolomics dataset supporting the conclusions of this article has been deposited to the EMBL-EBI MetaboLights database (DOI: 10.1093/nar/gkz1019, PMID:31691833) with the identifier MTBLS1476. The complete dataset can be accessed here: https://www.ebi.ac.uk/metabolights/MTBLS1476.

Competing interests

The authors declare that they have no competing interests.

Funding

This work was supported by NIH 1F32 CA213797 (S.B. Matthews), NIH R01 CA140985 (C.A.S.), the Breast Cancer Research Foundation (BCRF-16-072; C.A.S.), and NIH R01 CA164166 (P.S.M.).

Author Contributions

SBM, CAS and PSM designed research; SBM, LMF, AVW, JFS, and MJ performed research and analyzed data; SBM and CAS wrote the initial draft of the paper, SBM, CAS, PK., and PSM edited the paper.

Acknowledgments

We thank the University of Colorado School of Medicine Advanced Light Microscopy and Electron Microscopy Cores for their technical assistance and services. We thank the University of Colorado Cancer Center Flow Cytometry, Biorepository Core, and Tissue Culture Cores supported by P30CA046934. We thank Margo Schumann for assistance with mitochondrial quantitation.

Authors' information

[1] Department of Pathology, University of Colorado Anschutz Medical Campus, Aurora CO 80045. [2] Division of Medical Oncology, Department of Medicine, University of Colorado Anschutz Medical Campus, Aurora CO 80045. [3] Division of Endocrinology, Metabolism, and Diabetes, Department of Medicine, University of Colorado Anschutz Medical Campus, Aurora CO 80045.

References

1. Jatoi I, Chen BE, Anderson WF, Rosenberg PS. Breast cancer mortality trends in the United States according to estrogen receptor status and age at diagnosis. J Clin Oncol. 2007;25(13):1683-90.
2. Grodin JM, Siiteri PK, MacDonald PC. Source of estrogen production in postmenopausal women. J Clin Endocrinol Metab. 1973;36(2):207-14.
3. Siiteri PK. Adipose tissue as a source of hormones. Am J Clin Nutr. 1987;45(1 Suppl):277-82.
4. Santoro N, Randolph JF, Jr. Reproductive hormones and the menopause transition. Obstet Gynecol Clin North Am. 2011;38(3):455-66.
5. Collaborative Group on Hormonal Factors in Breast C. Type and timing of menopausal hormone therapy and breast cancer risk: individual participant meta-analysis of the worldwide epidemiological evidence. Lancet. 2019;394(10204):1159-68.
6. Morgan LR. Megestrol acetate v tamoxifen in advanced breast cancer in postmenopausal patients. Semin Oncol. 1985;12(1 Suppl 1):43-7.
7. Muss HB, Wells HB, Paschold EH, Black WR, Cooper MR, Capizzi RL, et al. Megestrol acetate versus tamoxifen in advanced breast cancer: 5-year analysis–a phase III trial of the Piedmont Oncology Association. J Clin Oncol. 1988;6(7):1098-106.
8. Bines J, Dienstmann R, Obadia RM, Branco LG, Quintella DC, Castro TM, et al. Activity of megestrol acetate in postmenopausal women with advanced breast cancer after nonsteroidal aromatase inhibitor failure: a phase II trial. Ann Oncol. 2014;25(4):831-6.
9. Long MD, Campbell MJ. Pan-cancer analyses of the nuclear receptor superfamily. Nucl Receptor Res. 2015;2.

10. Mohammed H, Russell IA, Stark R, Rueda OM, Hickey TE, Tarulli GA, et al. Progesterone receptor modulates ERalpha action in breast cancer. Nature. 2015;523(7560):313-7.
11. Singhal H, Greene ME, Tarulli G, Zarnke AL, Bourgo RJ, Laine M, et al. Genomic agonism and phenotypic antagonism between estrogen and progesterone receptors in breast cancer. Sci Adv. 2016;2(6):e1501924.
12. Finlay-Schultz J, Gillen AE, Brechbuhl HM, Ivie JJ, Matthews SB, Jacobsen BM, et al. Breast Cancer Suppression by Progesterone Receptors Is Mediated by Their Modulation of Estrogen Receptors and RNA Polymerase III. Cancer Res. 2017;77(18):4934-46.
13. Tidwell TR, Soreide K, Hagland HR. Aging, Metabolism, and Cancer Development: from Peto's Paradox to the Warburg Effect. Aging Dis. 2017;8(5):662-76.
14. Boonyaratanakornkit V, Pateetin P. The role of ovarian sex steroids in metabolic homeostasis, obesity, and postmenopausal breast cancer: molecular mechanisms and therapeutic implications. Biomed Res Int. 2015;2015:140196.
15. Klinge CM. Estrogenic control of mitochondrial function and biogenesis. J Cell Biochem. 2008;105(6):1342-51.
16. Horwitz KB, McGuire WL. Estrogen control of progesterone receptor in human breast cancer. Correlation with nuclear processing of estrogen receptor. J Biol Chem. 1978;253(7):2223-8.
17. Hilton HN, Doan TB, Graham JD, Oakes SR, Silvestri A, Santucci N, et al. Acquired convergence of hormone signaling in breast cancer: ER and PR transition from functionally distinct in normal breast to predictors of metastatic disease. Oncotarget. 2014;5(18):8651-64.
18. Forbes NS, Meadows AL, Clark DS, Blanch HW. Estradiol stimulates the biosynthetic pathways of breast cancer cells: detection by metabolic flux analysis. Metab Eng. 2006;8(6):639-52.
19. Pastorelli R, Carpi D, Airoldi L, Chiabrando C, Bagnati R, Fanelli R, et al. Proteome analysis for the identification of in vivo estrogen-regulated proteins in bone. Proteomics. 2005;5(18):4936-45.
20. Stirone CD, S.P.; Krause, D.N.; Procaccio, V.;. Estrogen increases mitochondrial efficiency and reduces oxidative stress in cerebral blood vessels. Molecular Pharmacology. 2005;68(4):959-65.
21. Yadav RN. Isocitrate dehydrogenase activity and its regulation by estradiol in tissues of rats of various ages. Cell Biochem Function. 1988;6(3):197-202.
22. Rivenzon-Segal D, Boldin-Adamsky S, Seger D, Seger R, Degani H. Glycolysis and glucose transporter 1 as markers of response to hormonal therapy in breast cancer. Int J Cancer. 2003;107(2):177-82.
23. Furman E, Rushkin E, Margalit R, Bendel P, Degani H. Tamoxifen induced changes in MCF7 human breast cancer: in vitro and in vivo studies using nuclear magnetic resonance spectroscopy and imaging. J Steroid Biochem Mol Biol. 1992;43(1-3):189-95.
24. Chen JQB, T. R.; Yager, D. R.; . Mechanisms of hormone carcinogenesis: evolution of views, roles of mitochondria. In: Berstein LRS, R. S.;, editor. Innovative Endocrinology of Cancer. Springer series: Advances in experimental medicine and biology. Austin, TX: Landes Bioscience / Springer Science+Business Media; 2008.

25. Chen JQ, Delannoy M, Cooke C, Yager JD. Mitochondrial localization of ERalpha and ERbeta in human MCF7 cells. Am J Physiol Endocrinol Metab. 2004;286(6):E1011-22.
26. Pedram A, Razandi M, Wallace DC, Levin ER. Functional estrogen receptors in the mitochondria of breast cancer cells. Mol Biol Cell. 2006;17(5):2125-37.
27. Richer JK, Jacobsen BM, Manning NG, Abel MG, Wolf DM, Horwitz KB. Differential gene regulation by the two progesterone receptor isoforms in human breast cancer cells. J Biol Chem. 2002;277(7):5209-18.
28. Schlaepfer IR, Hitz CA, Gijon MA, Bergman BC, Eckel RH, Jacobsen BM. Progestin modulates the lipid profile and sensitivity of breast cancer cells to docetaxel. Mol Cell Endocrinol. 2012;363(1-2):111-21.
29. Behera MA, Dai Q, Garde R, Saner C, Jungheim E, Price TM. Progesterone stimulates mitochondrial activity with subsequent inhibition of apoptosis in MCF-10A benign breast epithelial cells. Am J Physiol Endocrinol Metab. 2009;297(5):E1089-96.
30. Dai Q, Shah AA, Garde RV, Yonish BA, Zhang L, Medvitz NA, et al. A truncated progesterone receptor (PR-M) localizes to the mitochondrion and controls cellular respiration. Mol Endocrinol. 2013;27(5):741-53.
31. Kabos P, Finlay-Schultz J, Li C, Kline E, Finlayson C, Wisell J, et al. Patient-derived luminal breast cancer xenografts retain hormone receptor heterogeneity and help define unique estrogen-dependent gene signatures. Breast Cancer Res Treat. 2012;135(2):415-32.
32. Sartorius CA, Shen T, Horwitz KB. Progesterone receptors A and B differentially affect the growth of estrogen-dependent human breast tumor xenografts. Breast Cancer Res Treat. 2003;79(3):287-99.
33. Sartorius CA, Harvell DM, Shen T, Horwitz KB. Progestins initiate a luminal to myoepithelial switch in estrogen-dependent human breast tumors without altering growth. Cancer Res. 2005;65(21):9779-88.
34. Nemkov T, D'Alessandro A, Hansen KC. Three-minute method for amino acid analysis by UHPLC and high-resolution quadrupole orbitrap mass spectrometry. Amino Acids. 2015;47(11):2345-57.
35. Nemkov T, Hansen KC, D'Alessandro A. A three-minute method for high-throughput quantitative metabolomics and quantitative tracing experiments of central carbon and nitrogen pathways. Rapid Commun Mass Spectrom. 2017;31(8):663-73.
36. Gehrke S, Rice S, Stefanoni D, Wilkerson RB, Nemkov T, Reisz JA, et al. Red Blood Cell Metabolic Responses to Torpor and Arousal in the Hibernator Arctic Ground Squirrel. J Proteome Res. 2019.
37. Xia J, Psychogios N, Young N, Wishart DS. MetaboAnalyst: a web server for metabolomic data analysis and interpretation. Nucleic Acids Res. 2009;37(Web Server issue):W652-60.
38. Chong J, Soufan O, Li C, Caraus I, Li S, Bourque G, et al. MetaboAnalyst 4.0: towards more transparent and integrative metabolomics analysis. Nucleic Acids Res. 2018;46(W1):W486-W94.
39. Xia J, Wishart DS. Metabolomic data processing, analysis, and interpretation using MetaboAnalyst. Curr Protoc Bioinformatics. 2011;Chapter 14:Unit 14 0.
40. Finlay-Schultz J, Cittelly DM, Hendricks P, Patel P, Kabos P, Jacobsen BM, et al. Progesterone downregulation of miR-141 contributes to expansion of stem-like breast cancer cells through

maintenance of progesterone receptor and Stat5a. Oncogene. 2015;34(28):3676-87.
41. Bailey HH. L-S,R-buthionine sulfoximine: historical development and clinical issues. Chem Biol Interact. 1998;111-112:239-54.
42. Hernandez G, Thornton C, Stotland A, Lui D, Sin J, Ramil J, et al. MitoTimer: a novel tool for monitoring mitochondrial turnover. Autophagy. 2013;9(11):1852-61.
43. Pfaffl MW. A new mathematical model for relative quantification in real-time RT-PCR. Nucleic Acids Res. 2001;29(9):e45.
44. Liesa M, Shirihai OS. Mitochondrial dynamics in the regulation of nutrient utilization and energy expenditure. Cell Metab. 2013;17(4):491-506.
45. Martinez-Redondo V, Pettersson AT, Ruas JL. The hitchhiker's guide to PGC-1alpha isoform structure and biological functions. Diabetologia. 2015;58(9):1969-77.
46. Horwitz KB, Dye WW, Harrell JC, Kabos P, Sartorius CA. Rare steroid receptor-negative basal-like tumorigenic cells in luminal subtype human breast cancer xenografts. Proc Natl Acad Sci U S A. 2008;105(15):5774-9.
47. Kabos P, Haughian JM, Wang X, Dye WW, Finlayson C, Elias A, et al. Cytokeratin 5 positive cells represent a steroid receptor negative and therapy resistant subpopulation in luminal breast cancers. Breast Cancer Res Treat. 2011;128(1):45-55.
48. Goodman CR, Sato T, Peck AR, Girondo MA, Yang N, Liu C, et al. Steroid induction of therapy-resistant cytokeratin-5-positive cells in estrogen receptor-positive breast cancer through a BCL6-dependent mechanism. Oncogene. 2016;35(11):1373-85.
49. Fettig LM, McGinn O, Finlay-Schultz J, LaBarbera DV, Nordeen SK, Sartorius CA. Cross talk between progesterone receptors and retinoic acid receptors in regulation of cytokeratin 5-positive breast cancer cells. Oncogene. 2017;36(44):6074-84.
50. Truong TH, Dwyer AR, Diep CH, Hu H, Hagen KM, Lange CA. Phosphorylated Progesterone Receptor Isoforms Mediate Opposing Stem Cell and Proliferative Breast Cancer Cell Fates. Endocrinology. 2019;160(2):430-46.
51. Pei S, Minhajuddin M, Callahan KP, Balys M, Ashton JM, Neering SJ, et al. Targeting aberrant glutathione metabolism to eradicate human acute myelogenous leukemia cells. J Biol Chem. 2013;288(47):33542-58.
52. Mizuno T, Suzuki N, Makino H, Furui T, Morii E, Aoki H, et al. Cancer stem-like cells of ovarian clear cell carcinoma are enriched in the ALDH-high population associated with an accelerated scavenging system in reactive oxygen species. Gynecol Oncol. 2015;137(2):299-305.
53. Miran T, Vogg ATJ, Drude N, Mottaghy FM, Morgenroth A. Modulation of glutathione promotes apoptosis in triple-negative breast cancer cells. FASEB J. 2018;32(5):2803-13.
54. Santen RJ. Risk of breast cancer with progestins: critical assessment of current data. Steroids. 2003;68(10-13):953-64.

55. Horwitz KB, Sartorius CA. Progestins in hormone replacement therapies reactivate cancer stem cells in women with preexisting breast cancers: a hypothesis. J Clin Endocrinol Metab. 2008;93(9):3295-8.
56. Shyh-Chang N, Daley GQ, Cantley LC. Stem cell metabolism in tissue development and aging. Development. 2013;140(12):2535-47.
57. Batlle E, Clevers H. Cancer stem cells revisited. Nat Med. 2017;23(10):1124-34.
58. Alirol E, Martinou JC. Mitochondria and cancer: is there a morphological connection? Oncogene. 2006;25(34):4706-16.
59. Fu W, Liu Y, Yin H. Mitochondrial Dynamics: Biogenesis, Fission, Fusion, and Mitophagy in the Regulation of Stem Cell Behaviors. Stem Cells Int. 2019;2019:9757201.
60. Yu M, Chen S, Hong W, Gu Y, Huang B, Lin Y, et al. Prognostic role of glycolysis for cancer outcome: evidence from 86 studies. J Cancer Res Clin Oncol. 2019;145(4):967-99.
61. Havas KM, Milchevskaya V, Radic K, Alladin A, Kafkia E, Garcia M, et al. Metabolic shifts in residual breast cancer drive tumor recurrence. J Clin Invest. 2017;127(6):2091-105.

Supplementary Files Legends

Figure S1. Progestins do not increase expression of key fission machinery. T47D cells were treated with vehicle (0.2% EtOH), E2 (10^{-8} nM), R5020 (10^{-8} nM), or E2+R5020 (10^{-8} nM each) for the indicated timepoints and analyzed for fission machinery. A-C) Transcripts corresponding to key fission machinery were evaluated through qPCR. Primer sets are reported in **Table S3**. Values are mean ± SEM of ΔΔCt and represent at least 2 independent experiments. **P* <0.05, ***P* <0.01, ****P* <0.001 for the indicated comparisons using one-way ANOVA. *n.s.* = not significant. D-E) T47D cells were treated with vehicle (0.2% EtOH), E2 (10^{-8} nM), R5020 (10^{-8} nM), or E2+R5020 (10^{-8} nM each) for 24, 48, or 72 hrs. Lysates were collected and analyzed by immunoblot with 100 mg protein loaded per lane. Incubation with rabbit polyclonal antibody against phospho-Ser^{616} Drp-1 (1:1000) was followed by goat anti-rabbit fluorescent secondary. E) Incubation with mouse monoclonal antibody against Drp-1 (1:1000) was followed by goat anti-mouse fluorescent secondary. b-actin (1:2000) was used as a loading control for both antibodies. F) Protein levels for phospho-Se^{r616} Drp-1 and total Drp-1 were normalized to loading control then reported as the ratio of phospho:total Drp-1.

Figure S2. Progestin co-treatment with estrogen decreases mitochondrial biogenesis factors. Quantitative real-time PCR analysis of mitochondrial biogenesis machinery, including PGC family members, Nrf1, and mitochondrial transcription factor A (TFAM), on UCD65 cells treated with vehicle (0.2% EtOH), E2 (10^{-8} nM), R5020 (10^{-8} nM), or E2+R5020 (10^{-8} nM each). Values are mean ± SEM of ΔΔCt and represent at least 3 independent experiments. A-D) Statistical outcomes of comparisons between Veh vs. E2 and between E2 vs. E2+P are reported. For C), these comparisons were not significantly different. **P* <0.05, ***P* <0.01, ****P* <0.001 for the indicated comparisons using one-way ANOVA. *n.s.* = not significant.

Figure S3. Progestin co-treatment with estrogen mitigates E2-induced Nrf2 expression. T47D cells were treated with vehicle (0.2% EtOH), E2 (10^{-8} nM), R5020 (10^{-8} nM), or E2+R5020 (10^{-8} nM each) for 24 hrs. Lysates were collected and analyzed by immunoblot with 50 mg protein loaded per lane. Incubation with rabbit polyclonal antibody against Nrf2 (1:1000) was followed by goat anti-rabbit fluorescent secondary. a-tubulin (1:30000) was used as a loading control.

Figures

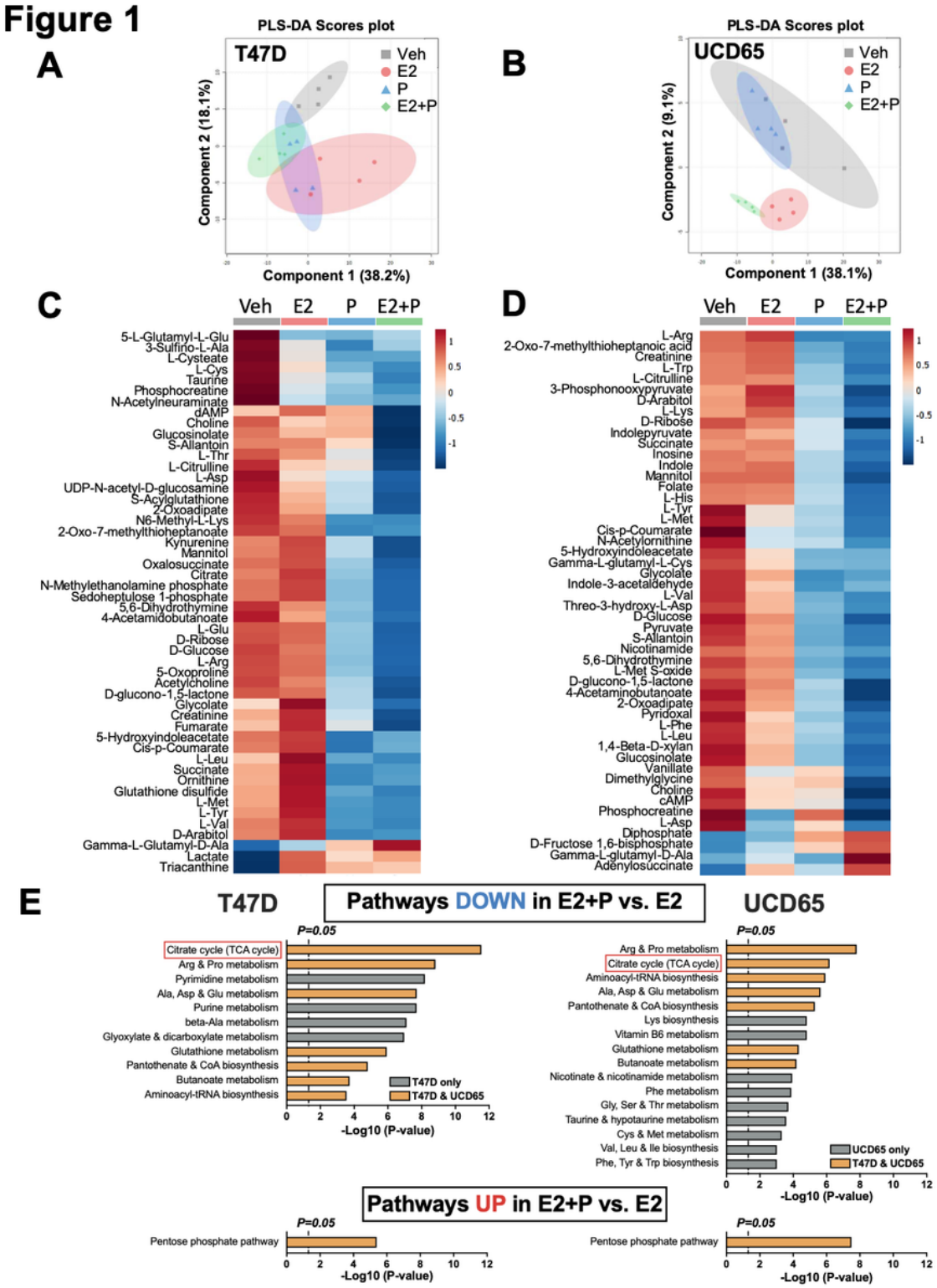

Figure 1

Progestins mitigate E2-driven metabolite changes. Partial least squares discriminant analysis (PLS-DA) scores plots of metabolomics data for A) T47D and B) UCD65 cells treated with vehicle (0.2% EtOH), E2 (10-8 nM), R5020 (10-8 nM), or E2+R5020 (10-8 nM each) for 24 h. C,D) Top 50 variables arranged in heatmaps (Pearson distance, average linkage, using PLS-DA variable importance scores). Pair-wise comparisons were performed for Veh vs. E2-treated cells and for E2 vs. E2+P-treated cells using random

forest analysis to identify important variables and analyzed via MetPA (P-value cutoff for enrichment, P < .05). E) Overlapping and (orange bars) unique (gray bars) pathways in T47D and UCD65 cells that are down in comparison of E2+P vs. E2 (top) or up in comparison of E2+P vs. E2 (bottom), with corresponding -log(10) P-values representing enrichment.

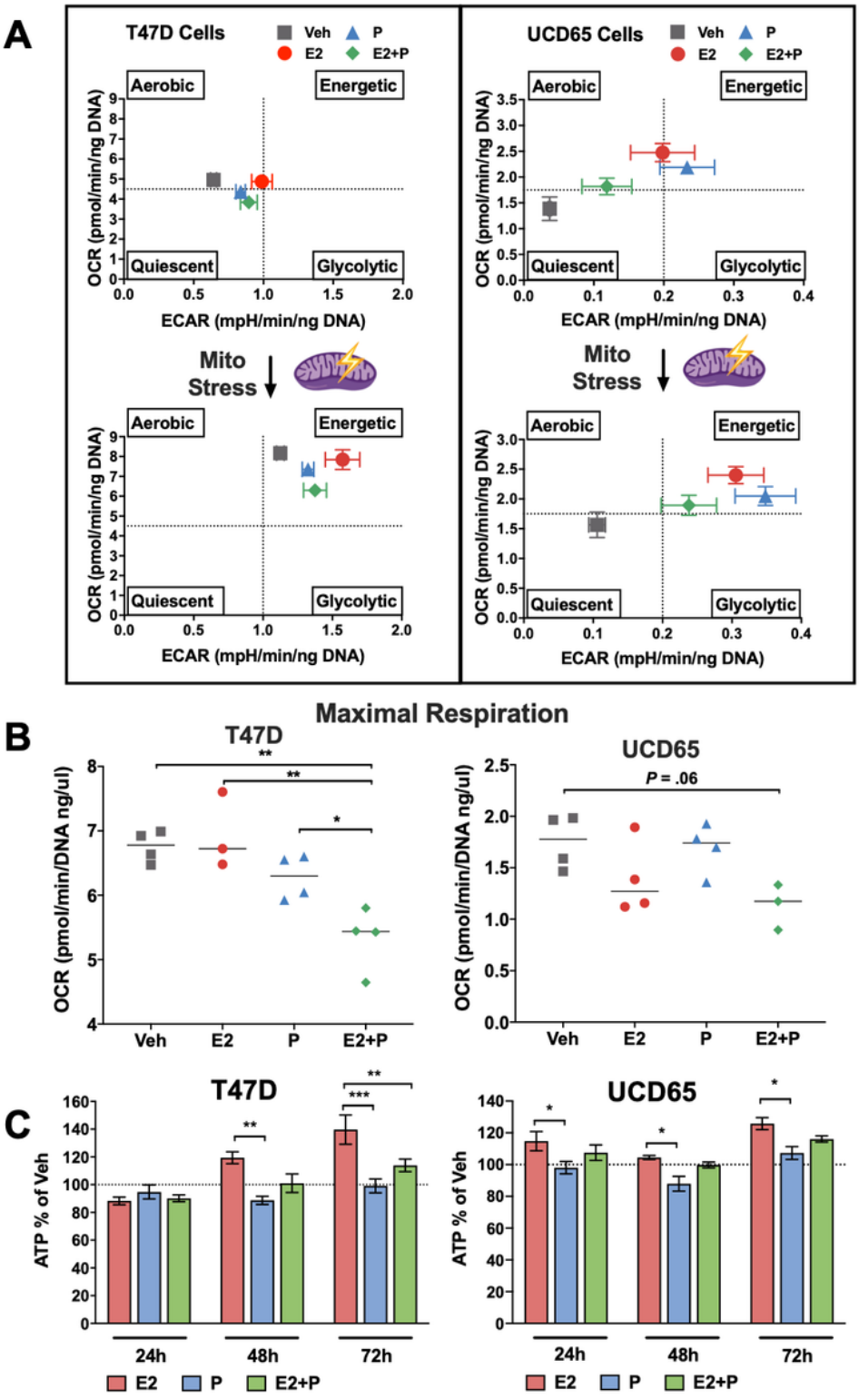

Figure 2

Progestin co-treatment with estrogen alters the cellular energetic phenotype. A) Energetic phenotype from Seahorse XF Bioanalyzer (Agilent) Mito Stress Test following 24 h (T47D, left) or 48 h (UCD65, right) treatment with vehicle (0.2% EtOH), E2 (10-8 nM), R5020 (10-8 nM), or E2+R5020 (10-8 nM each). Phenotype for both cell lines is shown under basal conditions (top) or following induction of mitochondrial stress with oligomycin (ATP synthase inhibitor) + FCCP (membrane uncoupler) (bottom). OCR = oxygen consumption rate; ECAR = extracellular acidification rate. B) Maximal respiration in response to FCCP stimulation from Mito Stress Test, where maximal respiration = peak OCR following FCCP – non-mitochondrial oxygen consumption. C) Time-course of intracellular ATP stores in response to hormone treatment. Values are means ± SEM of 3-4 technical replicates normalized to DNA content following the assay. *P < 0.05, **P <0.01, ***P <0.001 for the indicated comparisons using one-way ANOVA.

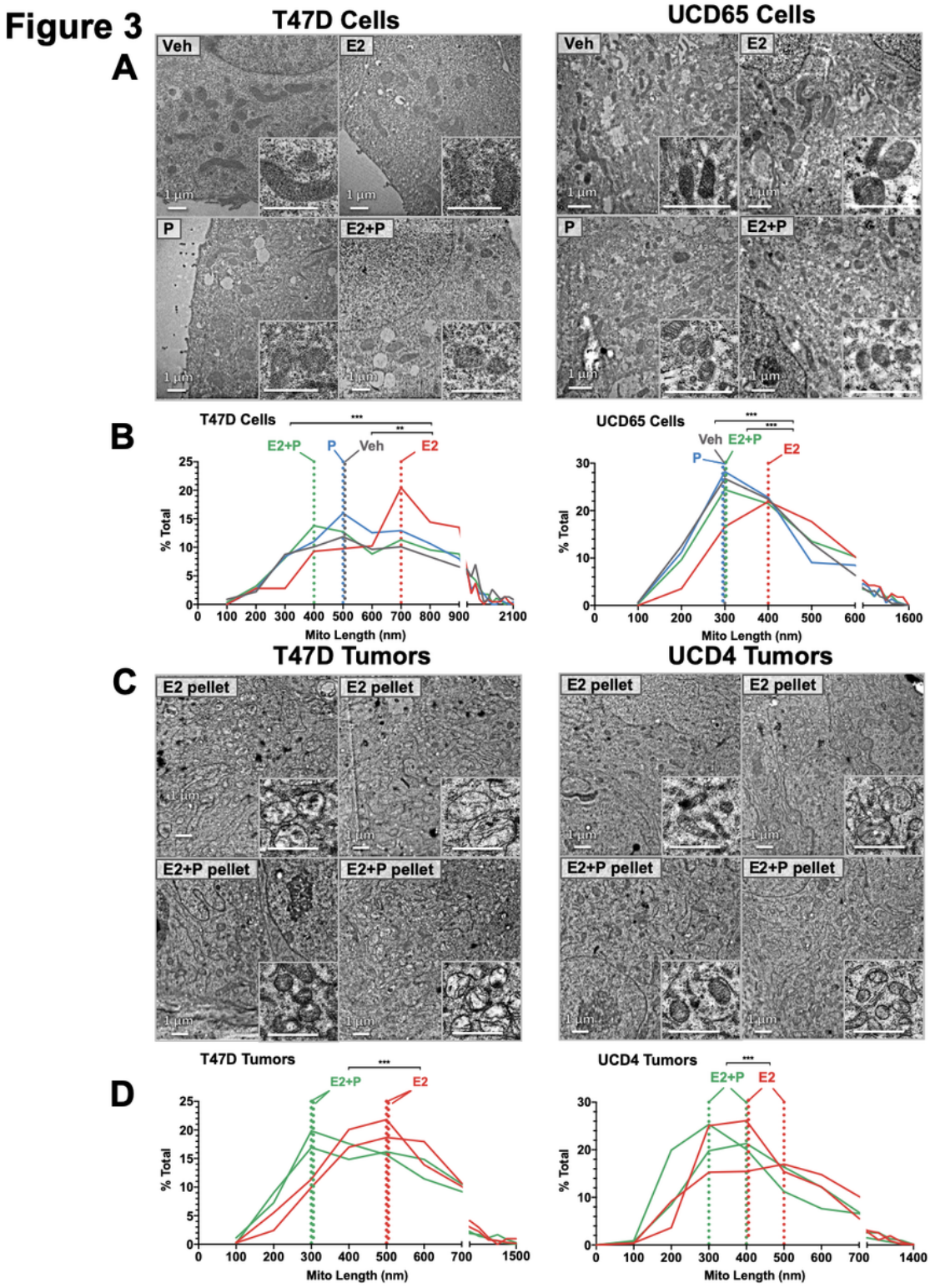

Figure 3

Progestins reduce mitochondrial length. A) Cultured T47D and UCD65 cells treated with vehicle (0.2% EtOH), E2 (10-8 nM), R5020 (10-8 nM), or E2+R5020 (10-8 nM each) and C) T47D and UCD4 tumor samples from mice with implanted hormone pellets containing E2 alone or E2+P4 were fixed, sectioned, and imaged using transmission electron microscopy. A representative image set is presented. B) Mitochondria length in cultured cells and D) tumor samples was measured along the longest axis in Fiji

in >200 mitochondria across 10-14 fields per treatment. Histograms represent mitochondrial length corresponding to 100-nm bins. *P <0.05, **P <0.01, ***P <0.001 for the indicated comparisons using Kolmogorov-Smirnov test for frequency distributions comparing Veh vs. E2 and comparing E2 vs. E2+P.

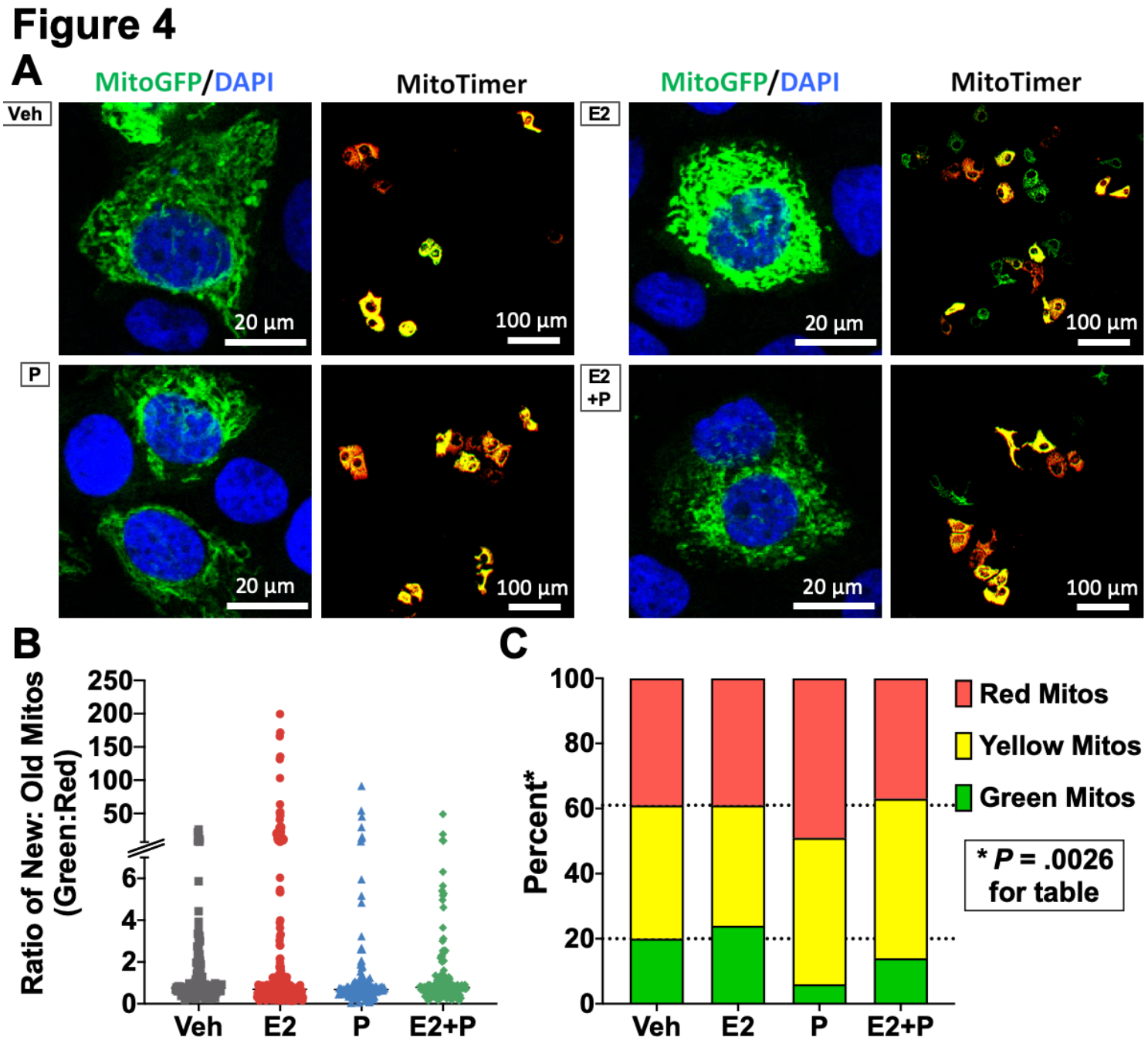

Figure 4

Progestin co-treatment with estrogen alters mitochondrial turnover. A) MitoGFP: Representative fields from laser scanning confocal images at 40X magnification on T47D cells treated with with vehicle (0.2% EtOH), E2 (10-8 nM), R5020 (10-8 nM), or E2+R5020 (10-8 nM each) for 48 h then labeled overnight with CellLights BacMam 2.0 MitoGFP (Thermo Fisher, Waltham, MA). Cells were fixed in paraformaldehyde, counterstained with DAPI, and mounted on coverslips. Images were collected using confocal laser scanning microscopy (Zeiss LSM 780) with 40X objective. MitoTimer: Representative fields from laser

scanning confocal images taken at 10X magnification on T47D cells stably transduced with the doxycycline-inducible MitoTimer construct. Cells were pulsed with doxycycline for 1 h, washed, treated with hormone for 48h, pulsed with Dox again, washout, and a final 24 h hormone treatment. B) Treated cells were fixed in 4% paraformaldehyde and imaged on an Olympus BX40 microscope at 10X magnification. Ratios of green to red fluorescent signal are shown and represent mean ± SEM of >200 cells across 5 fields per treatment. C) Intracellular ratios of red to green fluorescence were used to assign categorical cutoffs of predominantly red, green, or yellow mitochondria based on distribution of Veh-treated cells and shown as % of total. P = .0026 for the table using chi-square contingency analysis.

Figure 5

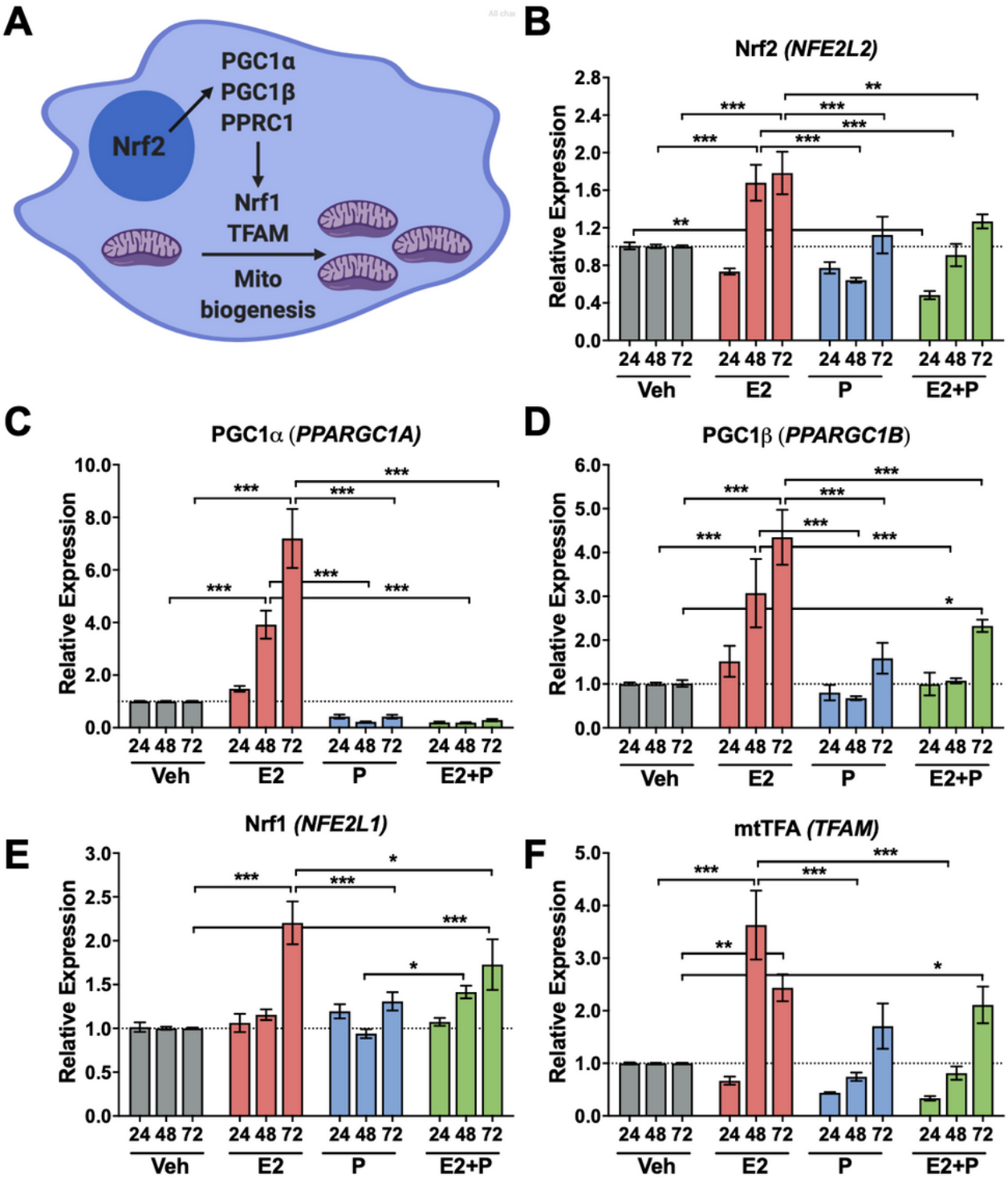

Figure 5

Progestin co-treatment decreases mitochondrial biogenesis factors. A) Cartoon of mitochondrial biogenesis schematic using BioRender (Toronto, Ontario). B-F) Quantitative real-time PCR analysis of mitochondrial biogenesis machinery, including PGC family members, Nrf1, and mitochondrial transcription factor A (TFAM), on T47D cells treated with vehicle (0.2% EtOH), E2 (10-8 nM), R5020 (10-8

nM), or E2+R5020 (10-8 nM each). Values are mean ± SEM of ΔΔCt and represent at least 4 independent experiments. *P <0.05, **P <0.01, ***P <0.001 for the indicated comparisons using one-way ANOVA.

Figure 6

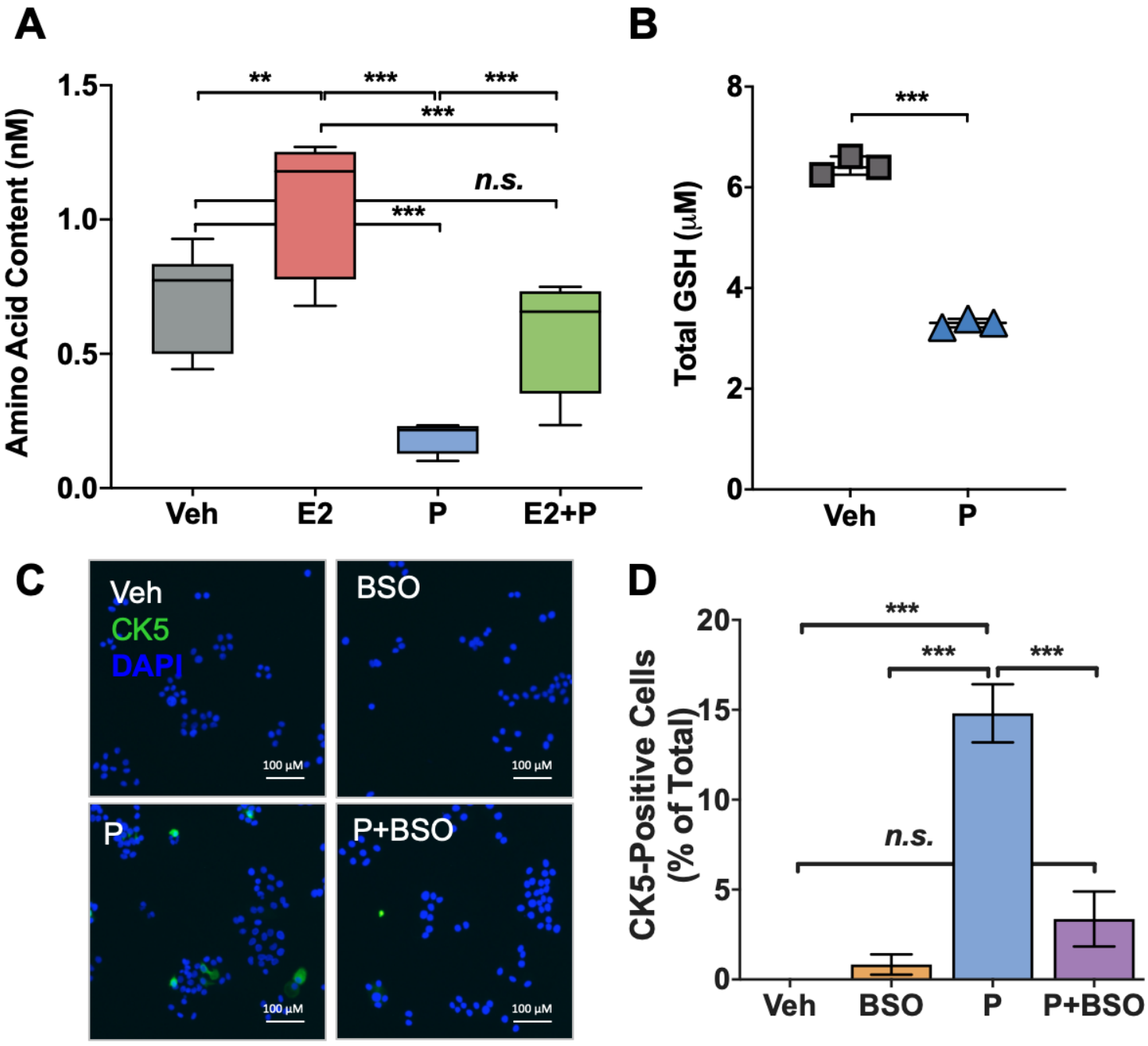

Figure 6

Hormonal regulation of amino acid pools reveals glutathione vulnerability in progestin-inducible cancer stem cells. T47D cells treated with vehicle (0.2% EtOH), E2 (10-8 nM), natural progesterone (P4) (10-7 nM), or E2+P4 (E2+P, 10-8 or 10-7 nM, respectively) for 24 hrs were lysed and evaluated for intracellular pools of A) amino acids and B) total glutathione (total glutathione - reduced (GSH) + oxidized (GSSG) glutathione). Values represent mean ± SEM of triplicate measures. C) T47D cells were treated with Veh,

P4, the glutathione synthesis inhibitor buthionine sulfoximine (BSO) (10-4 M), or P4+BSO for 48 hrs. Cells were fixed using methanol/acetone and immunocytochemistry (ICC) was performed against cytokeratin (CK)-5 (green) and counterstained with Dapi (blue). Representative panels are shown at 10X magnification. D) Percentage of CK5+ cells was quantified using ImageJ analysis of ICC images. Values are means ± SEM of 5 fields per treatment. *P <0.05, **P <0.01, ***P <0.001 for the indicated comparisons using one-way ANOVA. n.s. = not significant.

Supplementary Files

This is a list of supplementary files associated with this preprint. Click to download.

- FigS3.png
- SupplementaryMethods.docx
- SupplementaryTables.docx
- FigS1.png
- FigS2.png